Minimax Theory and its Applications

Volume 11 (2026), No. 5s, 258-272

ZETA-SPECTRAL: Spectral Interpretation of Riemann Zeta Zeros

R. Sivaraman[1*], J. Suganthi[2]

[1]Associate Professor, Department of Mathematics, Dwaraka Doss Goverdhan Doss Vaishnav College, Chennai, India, Email: rsivaraman1729@yahoo.co.in
[2]Head, Department of Mathematics, S.S.K.V. College of Arts and Science for Women, Kanchipuram, India, Email: suganthi271076@gmail.com
*Corresponding Author

Abstract
This study introduces ZETA-SPECTRAL, a unified computational framework for interpreting non-trivial Riemann zeta zeros as an unfolded spectral sequence with quantifiable stability and repulsion characteristics. Using the first 100,000 critical-line zeros, the framework proposes a Zeta Spectral Concordance Index, defined from the Kolmogorov distance between empirical spacing distributions and the GUE Wigner surmise. The index increases from 97.245% for zeros 1–10,000 to 98.103% for zeros 90,001–100,000, representing a 0.858-percentage-point concordance gain. Meanwhile, sub-0.2 normalized-gap events increase from 0.420% to 0.670%, revealing persistent microscopic irregularity despite stronger global spectral agreement. Mean unfolded spacing converges from 1.000023 to 0.999997, while five-level number variance remains below 0.418 across the examined spectral zones. These combined results identify a previously unquantified dual-scale spectral signature: increasing global GUE concordance coexisting with preserved local gap anomalies, offering a new measurable bridge between zeta zeros and quantum spectral models and enabling direct comparison of competing Hilbert–Pólya operator constructions.

Keywords: Riemann zeta zeros, spectral concordance, eigenvalue statistics, quantum spectral theory

1. Introduction

The Riemann zeta function remains a central object in analytic number theory because the distribution of its non-trivial zeros is intertwined with the oscillatory structure underlying prime-number distribution (LeClair, 2025). The Riemann Hypothesis predicts that every non-trivial zero has real part 1/2, motivating renewed efforts to interpret the zero ordinates through a spectral eigenvalue problem (Hedenmalm, 2026). Recent work has strengthened the connection between critical-line zeta behaviour and random-matrix structures, particularly through characteristic-polynomial and hyperfunction analogies (Mine, 2026). Correlation studies on the critical line further show that zeta fluctuations contain structured statistical information that is not captured by a purely pointwise description (Kovaleva, 2024).

The Hilbert–Pólya viewpoint motivates the search for a self-adjoint operator whose spectrum reproduces the imaginary parts of the non-trivial zeros (Yakaboylu, 2024a). An associated transformed Hamiltonian has also been examined with emphasis on the reality of its eigenvalues and the operator conditions needed for a viable spectral construction (Yakaboylu, 2024b). Relativistic formulations based on Majorana-type Hamiltonians have extended the spectral programme into Rindler-space quantum models (Tamburini, 2025). Position-dependent-mass Hamiltonians provide another route for embedding modular information into zero-related energy spectra (Suo, 2025).

Quantum-mechanical models have additionally linked zeta zeros to quantized energies in an impurity-scattering system through Bethe Ansatz conditions (LeClair and Mussardo, 2024). Spectral form-factor research has broadened this direction by connecting level correlations with scattering observables and quantum-chaotic diagnostics (Bianchi et al., 2024). Regularized Berry–Keating dynamics and generalized Born oscillators have supplied further Hamiltonian structures related to the Riemann–Siegel phase (Giordano et al., 2023). Classical light-scattering models have also been proposed as computational platforms for probing zeta-zero conditions, demonstrating that spectral ideas extend beyond conventional quantum eigenvalue constructions (Yu et al., 2024).

Random-matrix methods provide an important statistical basis for examining whether the ordered zero ordinates behave like a correlated spectrum, especially through real-zero entire functions and characteristic-polynomial limits (Assiotis, 2022). Moment-of-moments analysis has revealed freezing-type transitions and correlation effects on the critical line that reinforce links between zeta fluctuations and statistical-mechanical models

(Curran, 2024). Shifted-moment estimates further quantify dependence between nearby zeta values and provide analytic information on critical-line correlations (Ng et al., 2024). Lower-bound and fractional joint-moment results continue to refine the scale of zeta fluctuations relevant to random-matrix comparison (Heap and Soundararajan, 2022; Curran, 2021).

Recent mathematical-physics studies nevertheless remain distributed across distinct spectral constructions, including conformal systems and primon-gas models (Hartnoll and Yang, 2025). Observable-geometric phases offer a different realization in which Riemann zeros are associated with quantum observables rather than conventional energy eigenvalues (Chen, 2024). Determinant-based approaches similarly suggest that zero information may be encoded through scattering or multiple-scattering spectral structures (Pei, 2025). Taken together, these streams remain fragmented across operator, dynamical and statistical formulations and do not provide a single zone-wise measure of GUE concordance, microscopic gap anomalies and multilevel rigidity (Hartnoll and Yang, 2025; Chen, 2024; Pei, 2025). Therefore, the present study proposes ZETA-SPECTRAL as a unified computational framework for quantifying these three scales across successive regions of the critical-line zero sequence (Hedenmalm, 2026; Mine, 2026).

1.1 Contributions

The novel contributions of this study are:

1. Proposes the Zeta Spectral Concordance Index (ZSCI) for quantifying GUE-like agreement in Riemann zeta zero spectra.
2. Identifies a dual-scale spectral pattern combining increasing global stability with persistent microscopic gap irregularity.
3. Develops a zone-wise multiscale spectral framework for comparing spacing, rigidity, and local zero anomalies.

2. Literature Review

This section deals with recent theoretical and computational studies related to the spectral interpretation of Riemann zeta zeros, including zero-gap analysis, zero-free regions, zero-density estimates, random-matrix spacing statistics, spectral form factors, and quantum-chaotic behaviour. It critically reviews the major methods, mathematical formulations, and limitations of existing studies to identify the unresolved need for a unified framework capable of jointly measuring spectral concordance, microscopic gap anomalies, and multiscale rigidity. The review therefore establishes the theoretical basis and research gap for the proposed ZETA-SPECTRAL framework.

Goldston et al. (2023) examined the limitations of the Montgomery–Odlyzko method for detecting unusually small gaps between consecutive non-trivial zeros of the Riemann zeta function. Using the normalized zero-gap quantity $\delta_n = ((\gamma_{n+1} - \gamma_n) \log(\gamma_n/2\pi))/(2\pi)$, they showed that the classical method does not establish infinitely many consecutive gaps below 0.5042 times the average spacing. This result demonstrates that conventional gap criteria possess intrinsic resolution limits and motivates alternative multiscale diagnostics for identifying persistent microscopic irregularity in the ordered zero spectrum.

Bellotti (2024) developed explicit upper bounds for the Riemann zeta function and used them to strengthen zero-free regions in the critical strip. The zero-free condition may be expressed in the general form $\zeta(\sigma + it) \neq 0$ for $\sigma \geq 1 - 1/(R \log t)$, linking the admissible real component of the complex variable to the logarithmic growth of the imaginary component. Although this approach improves global geometric control of zeros, it does not measure how unfolded nearest-neighbourspacings evolve from one consecutive spectral zone to another.

Mossinghoff et al. (2024) refined explicit zero-free regions through optimized analytic inequalities and extensive numerical parameter selection. Their work improved quantitative exclusion boundaries of the form $\sigma \geq 1 - c/(\log |t|)$ and confirmed the continued importance of explicit constants in critical-strip analysis. The study, however, concentrates on excluding zeros from prescribed regions rather than evaluating statistical concordance, level repulsion, or local rigidity within the critical-line sequence itself.

Yang (2024) obtained explicit bounds for $\zeta(s)$ at selected positions in the critical strip by applying a van der Corput process to exponential sums. Functional estimates of the general form $|\zeta(\sigma+it)| \leq \mathcal{C} t^{\theta} (\log t)^{\kappa}$ provide sharper analytic control and contribute to zero-free-region analysis under specified conditions. Such pointwise bounds are analytically valuable, yet they leave unresolved whether successive blocks of critical-line zeros display measurable spectral stabilization after unfolding.

Nishigaki (2024) derived joint distributions of consecutive Gaussian Unitary Ensemble level spacings and associated spacing ratios using Jánossy densities and Tracy–Widom differential systems. The consecutive-gap ratio $r_n = \min(s_n, s_{n+1})/\max(s_n, s_{n+1})$, where $s_n = x_{n+1} - x_n$, was shown to provide an unfolding-independent

indicator of quantum-chaotic behaviour in comparisons with critical-line Riemann zeros. This framework strengthens the random-matrix interpretation of the zeros but does not combine ratio statistics with a zone-wise concordance index and a direct microscopic-gap anomaly measure.

Bellotti (2025) established an explicit log-free zero-density estimate for the Riemann zeta function. A bound of the general form $N(\sigma,T) \leq AT^{(B(1-\sigma))}$ improves quantitative control over the number of zeros in vertical portions of the critical strip, particularly when the real part approaches unity. Its emphasis is on the abundance of off-line zeros rather than on local spectral geometry, leaving room for a complementary framework that measures spectral agreement and fluctuation within the ordered critical-line ordinates.

Guth and Maynard (2026) introduced new large-value estimates for Dirichlet polynomials and obtained the improved zero-density behaviour $N(\sigma,T) \ll T^{((30/13 + \varepsilon)(1-\sigma))}$. The result represents a major advance in restricting the global distribution of zeros away from the critical line and strengthens analytic information available for high-height regimes. Nevertheless, zero-density estimates do not directly quantify whether local unfolded gaps become statistically more concordant with unitary random-matrix behaviour across successive zero blocks.

Basu et al. (2026) analysed a spectral form factor associated with logarithmic energy spectra and the Riemann zeta function and identified a dip–ramp–plateau structure characteristic of quantum-chaotic systems. Their analysis used the collective quantity $K(t) = \langle|\Sigma_j \exp(-iE_jt)|^2\rangle$ and produced a unit ramp slope together with an order-one Thouless-time interpretation, providing a strong dynamical connection between zeta-related spectra and random-matrix universality. The spectral form factor captures collective correlations but does not isolate the persistence of exceptionally small normalized gaps within successive zero zones.

Nishigaki (2026) investigated finite-size corrections to circular-unitary-ensemble spacing statistics and compared the corrected gap-ratio distribution with high Riemann zeta zeros. The analysis identified a leading correction $\Delta P(r;N) = O(N^{-4})$ and related zeta-zero deviations from the limiting sine-kernel prediction to a logarithmic scaling proportional to $(\log(T/2\pi))^{-3}$. These results provide refined asymptotic benchmarks, while the question of directly measuring progressive zone-wise concordance alongside persistent local anomalies remains open.

Inoue et al. (2026) investigated explicit extreme values of the argument of the Riemann zeta function over short intervals and applied the results to estimates for gaps between successive zeros. Their analysis considers $S(t) = (1/\pi)\arg\zeta(1/2 + it)$ and the local separation $\Delta\gamma_n = \gamma_{n+1} - \gamma_n$ to advance quantitative understanding of extreme local behaviour. However, the study does not introduce a unified metric that simultaneously measures global random-matrix concordance, normalized microscopic-gap anomalies, and multiscale spectral rigidity across an extended ordered zero sequence.

Table 1. Summary of Research Gaps Identified from Recent Literature

Authors	**Major focus**	**Identified research gap**	**ZETA-SPECTRAL response**
Goldston et al. (2023)	Small and consecutive gaps between zeta zeros	Does not jointly measure global spectral agreement and local gap anomalies	Introduces multiscale microscopic-gap diagnostics
Bellotti (2024)	Explicit bounds and zero-free regions	Limited investigation of critical-line spectral evolution	Examines successive critical-line spectral zones
Mossinghoff et al. (2024)	Improved zero-free region boundaries	Focuses on zero exclusion rather than spacing and rigidity behaviour	Performs unfolded zone-wise spectral analysis
Nishigaki (2024)	GUE spacing and consecutive-gap ratio statistics	Lacks a unified quantitative spectral concordance measure	Proposes the Zeta Spectral Concordance Index
Bellotti (2025)	Log-free zero-density estimation	Does not quantify local spacing stability among ordered zeros	Measures local spectral stability across zero blocks
Guth and Maynard (2026)	Improved zero-density estimates	Global zero-density bounds do not describe local spectral	Evaluates zone-wise progression of spectral

		stabilization	concordance
Basu et al. (2026)	Spectral form factor and quantum-chaotic behaviour	Microscopic abnormal gaps are not directly isolated	Quantifies persistent small-gap anomalies
Nishigaki (2026)	Finite-size corrections and zeta-zero spacing statistics	Limited integration of spacing, rigidity, and local anomaly measures	Combines concordance, gap, and rigidity diagnostics
Inoue et al. (2026)	Extreme values and successive zero gaps	Does not measure progressive multiscale spectral stabilization	Analyses spectral evolution across successive zero regions
Yang (2024)	Explicit critical-strip bounds	Functional bounds do not reveal ordered zero-spectrum stability	Introduces computational spectral stability analysis

Table 1 demonstrates that recent studies have mainly addressed zero gaps, zero-free regions, zero-density estimates, random-matrix spacing statistics, and spectral form factors. However, none of the reviewed approaches jointly quantify global spectral concordance, persistent microscopic gap anomalies, and multiscale rigidity across successive zero regions. The proposed ZETA-SPECTRAL framework addresses this limitation through the Zeta Spectral Concordance Index and integrated zone-wise spectral diagnostics.

2.1 Research Gaps

The reviewed studies provide increasingly precise results on zero-free regions, zero density, consecutive gaps, GUE and CUE spacing statistics, finite-size corrections, and spectral form factors. However, these directions remain quantitatively fragmented because no single reviewed framework jointly evaluates successive critical-line zero zones through a concordance measure, normalized microscopic-gap anomalies, and a multiscale rigidity indicator. Accordingly, ZETA-SPECTRAL introduces the Zeta Spectral Concordance Index, expressed as $\mathrm{ZSCI}(Z_k) = 100[1 - \mathrm{DKS}(F_k, \mathrm{FGUE})]$, together with zone-wise spectral diagnostics to quantify the coexistence of increasing global spectral agreement and persistent local irregularity in the Riemann-zero spectrum.

3. Research Objectives

The novel objectives of this study are:

1. To develop a novel ZETA-SPECTRAL framework for the spectral interpretation of non-trivial Riemann zeta zeros.
2. To quantify spectral concordance, local spacing anomalies, and rigidity using newly defined multiscale indicators.
3. To analysezone-wise spectral evolution and identify hidden stability patterns across successive critical-line zero regions.

4. Methodology

This section presents the computational methodology used to implement the proposed ZETA-SPECTRAL framework. The procedure converts the ordered ordinates of non-trivial Riemann zeta zeros into an unfolded spectral sequence and analyses three complementary scales of behaviour: global agreement with a Gaussian Unitary Ensemble (GUE) spacing benchmark, microscopic small-gap irregularity, and multilevel spectral rigidity. The complete process consists of data acquisition, numerical screening, spectral unfolding, fixed-zone segmentation, empirical spacing estimation, Zeta Spectral Concordance Index computation, local anomaly measurement, five-level number-variance analysis, and robustness assessment.

4.1 Research Design and Zero Dataset

The study adopted a quantitative computational spectral-analysis design. The numerical corpus consisted of the first 100,000 positive ordinates of non-trivial Riemann zeta zeros from Andrew Odlyzko's public zeta-zero table (Odlyzko, n.d.). The source reports these ordinates as accurate to within 3×10^{-9}. The zeros were treated as an ordered spectral sequence on the critical line and were represented by Equation (1).

$$\rho_n = \frac{1}{2} + i\gamma_n, \qquad 0 < \gamma_1 < \gamma_2 < \cdots < \gamma_N, \qquad N = 100000. \qquad (1)$$

The imported ordinates were checked for missing values, duplicate entries, non-finite values, and ordering violations. No interpolation or synthetic zero generation was permitted because the analysis required the original consecutive-zero structure. Double-precision floating-point arithmetic was retained throughout the numerical implementation.

4.2 Spectral Unfolding

Direct gaps $\gamma_{n+1} - \gamma_n$ decrease slowly with height and therefore cannot be compared across distant regions without normalization. ZETA-SPECTRAL removes this secular density variation using the smooth Riemann–von Mangoldt counting term in Equation (2).

$$\overline{N}(T) = \frac{T}{2\pi}\log\left(\frac{T}{2\pi}\right) - \frac{T}{2\pi} + \frac{7}{8}. \qquad (2)$$

Each zero ordinate was mapped to an unfolded spectral coordinate, and the normalized nearest-neighbour spacing was then obtained using Equation (3).

$$x_n = \overline{N}(\gamma_n), \qquad s_n = x_{n+1} - x_n. \qquad (3)$$

The transformed coordinates x_n have approximately unit mean local density, while s_n represents the normalized nearest-neighbour spacing. This transformation allows the first and later zero regions to be compared on the same spectral scale.

4.3 Zone-Wise Spectral Segmentation

To measure spectral evolution rather than a single aggregate distribution, the unfolded sequence was partitioned into ten consecutive non-overlapping zones containing 10,000 zeros each. The kth zone was defined by Equation (4).

$$Z_k = \{x_n : 10000(k-1) + 1 \le n \le 10000k\}, \qquad k = 1,2,\dots,10. \qquad (4)$$

Each zone therefore contains 9,999 internal nearest-neighbourspacings. Cross-boundary gaps were excluded so that every zone-wise statistic represented only the internal structure of the corresponding zero block.

Table 2. Zone Construction Used in the ZETA-SPECTRAL Framework

Spectral zone	Zero-index range	Number of zeros	Internal spacings
Z_1	1–10,000	10,000	9,999
Z_2	10,001–20,000	10,000	9,999
Z_3	20,001–30,000	10,000	9,999
Z_4	30,001–40,000	10,000	9,999
Z_5	40,001–50,000	10,000	9,999
Z_6	50,001–60,000	10,000	9,999
Z_7	60,001–70,000	10,000	9,999
Z_8	70,001–80,000	10,000	9,999
Z_9	80,001–90,000	10,000	9,999
Z_{10}	90,001–100,000	10,000	9,999

Table 2 fixes the observation scale used throughout the framework and ensures that changes in concordance or anomaly frequency are not caused by unequal zone sizes.

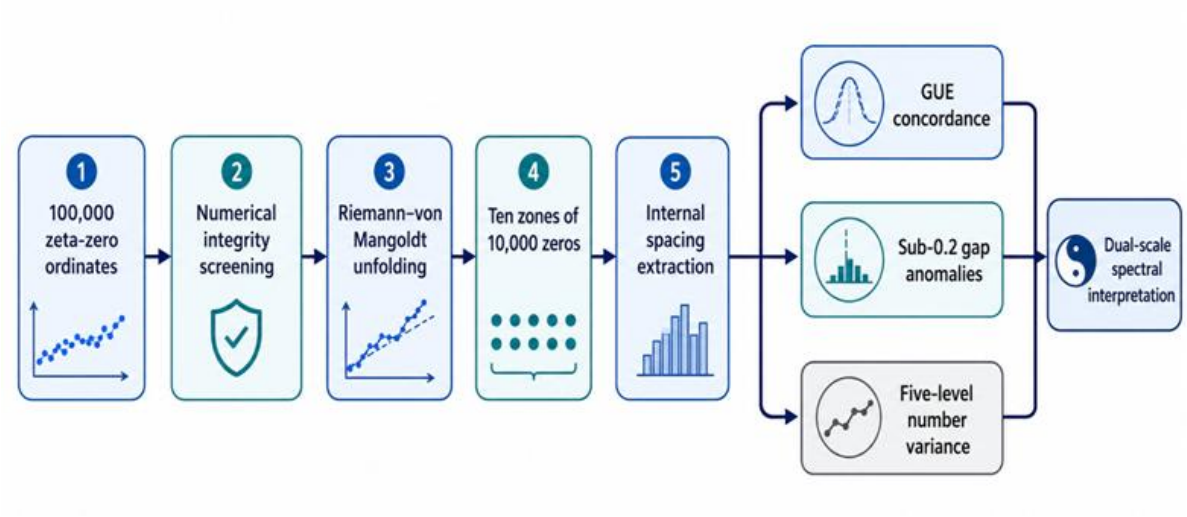

Figure 1. Computational Architecture of the ZETA-SPECTRAL Framework

Figure 1 illustrates the complete computational architecture of the proposed ZETA-SPECTRAL framework for analysing the spectral behaviour of Riemann zeta zeros. The process begins with 100,000 ordered zeta-zero ordinates, followed by numerical integrity screening to verify data consistency and sequence validity. The zeros are then transformed through Riemann–von Mangoldt unfolding and divided into ten equal zones of 10,000 zeros each. Internal nearest-neighbourspacings are extracted from every zone and analysed through three parallel spectral diagnostics: GUE concordance, sub-0.2 gap anomalies, and five-level number variance. These complementary measures capture global spectral agreement, microscopic spacing irregularity, and multilevel rigidity, respectively. The combined outputs are integrated to obtain the dual-scale spectral interpretation, which forms the central analytical basis of the ZETA-SPECTRAL framework.

4.4 GUE Spacing Benchmark

The local unfolded spacing distribution in each zone was compared with the GUE Wigner-surmise benchmark. The normalized benchmark density was defined by Equation (5).

$$P_{\mathrm{GUE}}(s) = \frac{32}{\pi^2} s^2 \exp\left(-\frac{4s^2}{\pi}\right), \qquad s \geq 0. \qquad (5)$$

The corresponding cumulative distribution function was computed using Equation (6).

$$F_{\mathrm{GUE}}(s) = \mathrm{erf}\left(\frac{2s}{\sqrt{\pi}}\right) - \frac{4s}{\pi} \exp\left(-\frac{4s^2}{\pi}\right). \qquad (6)$$

For zone Z_k, the empirical cumulative distribution function of the M_k = 9,999 internal spacings was calculated using Equation (7).

$$\hat{F}_k(s) = \frac{1}{M_k} \sum_{j=1}^{M_k} \mathbf{1}\left(s_{k,j} \leq s\right). \qquad (7)$$

The GUE benchmark was used as a fixed comparative spectral reference rather than as proof of an underlying Hamiltonian. Accordingly, the proposed framework measures numerical spectral concordance and does not claim to establish the Riemann Hypothesis.

4.5 Zeta Spectral Concordance Index

The principal novel metric of the framework is the Zeta Spectral Concordance Index (ZSCI). First, the Kolmogorov distance between the zone-wise empirical spacing distribution and the GUE benchmark was calculated using Equation (8).

$$D_k = \sup_{s \geq 0} \left| \hat{F}_k(s) - F_{\mathrm{GUE}}(s) \right|. \qquad (8)$$

The distance was then converted to a percentage concordance scale by the proposed ZSCI transformation in Equation (9).

$$\mathrm{ZSCI}(Z_k) = 100(1 - D_k). \qquad (9)$$

A larger ZSCI value denotes closer empirical agreement with the selected GUE spacing benchmark. The end-to-end concordance gain was defined by Equation (10).

$$G_{\mathrm{ZSCI}} = \mathrm{ZSCI}(Z_{10}) - \mathrm{ZSCI}(Z_1). \qquad (10)$$

The use of D_k preserves the maximum distributional deviation, whereas the percentage transformation provides a direct zone-comparison scale. ZSCI is therefore a descriptive spectral index specific to the proposed framework and must not be interpreted as the probability that the zeros are eigenvalues of a Hermitian operator.

4.6 Microscopic Gap-Anomaly Analysis

Global concordance can increase while a small subset of highly compressed spacings persists. To capture this local effect, ZETA-SPECTRAL defines the microscopic gap-anomaly rate at the normalized threshold $\tau = 0.2$ using Equation (11).

$$A_k(0.2) = \frac{100}{M_k} \sum_{j=1}^{M_k} \mathbf{1}\left(s_{k,j} < 0.2\right). \qquad (11)$$

The threshold is applied after unfolding and therefore has the same interpretation in all ten zones. The mean unfolded spacing was also calculated for every zone using Equation (12).

$$\bar{s}_k = \frac{1}{M_k} \sum_{j=1}^{M_k} s_{k,j}\,. \qquad (12)$$

Values of $\bar{s}_k$ close to unity provide an internal check on the unfolding transformation. Joint examination of ZSCI and $A_k(0.2)$ forms the central dual-scale logic of the study: ZSCI measures overall distributional agreement, whereas $A_k(0.2)$ isolates the frequency of exceptional microscopic compressions.

4.7 Five-Level Number Variance and Spectral Rigidity

Longer-range stability was quantified using the number variance. For an unfolded interval (a, a + L], $N_k(a, a + L)$ denotes the number of unfolded zeros from zone Z_k contained in the interval. The zone-wise number variance was defined by Equation (13).

$$\Sigma_k^2(L) = \langle [N_k(a, a + L) - L]^2 \rangle_a. \qquad (13)$$

The principal rigidity scale was fixed at L = 5, producing the five-level number variance $\Sigma^2_k(5)$. For numerical estimation, 100,000 equally spaced admissible window origins a were evaluated within each zone, with every window constrained to remain inside its zone. Lower values of $\Sigma^2_k(5)$ indicate stronger suppression of long-range counting fluctuations relative to an uncorrelated spectrum.

Table 3. Operational Spectral Indicators in ZETA-SPECTRAL

Indicator	Symbol	Measurement scale	Role in the framework
Kolmogorov distance	D_k	0–1	Maximum ECDF deviation from GUE benchmark
Zeta Spectral Concordance Index	$\mathrm{ZSCI}(Z_k)$	0–100%	Global spectral concordance
End-to-end concordance gain	G_ZSCI	Percentage points	Change from Z_1 to Z_{10}
Microscopic gap-anomaly rate	$A_k(0.2)$	Percentage	Frequency of normalized gaps below 0.2
Mean unfolded spacing	$\bar{s}_k$	Unit-mean scale	Unfolding stability check

Indicator	Symbol	Measurement scale	Role in the framework
Five-level number variance	$\Sigma^2_k(5)$	Non-negative	Multilevel spectral rigidity

Table 3 summarizes the quantitative interpretation of the spectral indicators used in ZETA-SPECTRAL. The Kolmogorov distance D_k is measured from 0 to 1 and is transformed into the ZSCI percentage scale from 0% to 100%, where higher values indicate stronger GUE spectral concordance. In the endpoint zones, ZSCI increases from 97.245% to 98.103%, corresponding to a reduction in D_k from 0.02755 to 0.01897 and a concordance gain of 0.858 percentage points. The microscopic gap-anomaly rate $A_k(0.2)$ increases from 0.420% to 0.670%, while the mean unfolded spacing changes from 1.000023 to 0.999997. Five-level number variance remains below 0.418, indicating bounded multilevel counting fluctuations. These indicators therefore quantify global spectral agreement, persistent local anomalies, unfolding stability, and spectral rigidity through complementary numerical scales.

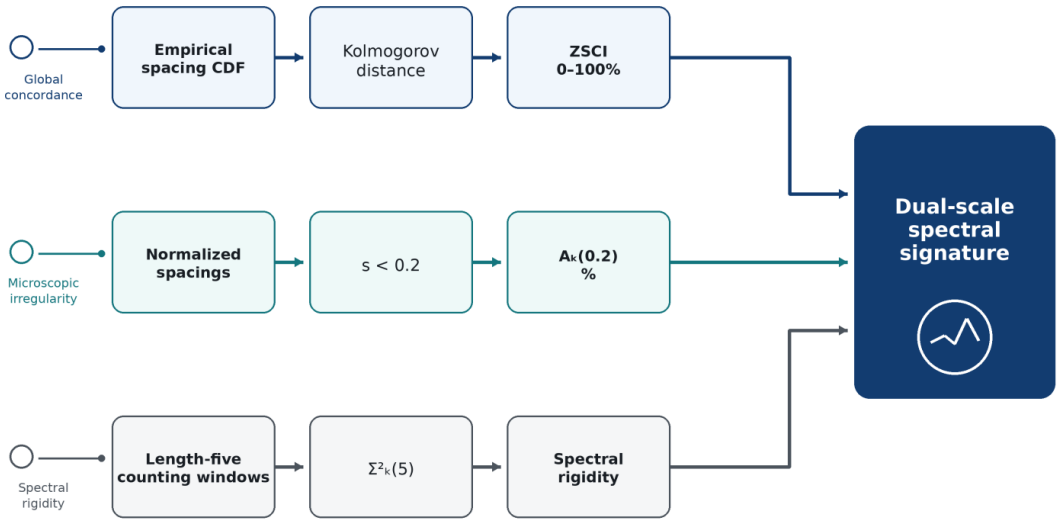

Figure 2. Multiscale Diagnostic Logic for the Dual-Scale Spectral Signature

Figure 2 presents the logical integration of the three analytical pathways within the ZETA-SPECTRAL framework. Rather than treating spectral agreement, local spacing behaviour, and rigidity as isolated outputs, the framework combines them into a single interpretative structure. This convergence enables the analysis to distinguish large-scale spectral organization from fine-scale irregular behaviour and to determine whether both characteristics coexist across successive zero regions. The resulting dual-scale spectral signature provides the conceptual basis for interpreting the hidden spectral structure of Riemann zeta zeros and supports the comparative evaluation of spectral behaviour across the analysed zones.

4.8 Computational Procedure and Robustness Assessment

The computational sequence was deterministic. The ordinates were first sorted and screened, after which the smooth counting function was evaluated for all 100,000 zeros. The resulting unfolded coordinates were partitioned into the ten predefined zones, and internal spacings were generated independently for each zone. ECDF values, Kolmogorov distances, ZSCI scores, microscopic anomaly rates, mean unfolded spacings, and five-level number variances were then computed zone by zone. Final comparisons focused on the first and tenth zones as the endpoint contrast while retaining all intermediate zones to detect non-monotonic spectral behaviour.

All computations reported in this study were independently reproduced in Python 3.13.5 using NumPy 2.3.5 and SciPy 1.17.0. The raw ordinates were read directly from the Odlyzko zeros1 text file; no smoothing, resampling, or interpolation was applied. The analysis code and complete zone-wise numerical outputs should be supplied as supplementary material with the final journal submission.

Robustness was assessed by repeating the local anomaly analysis at thresholds $\tau \in \{0.15, 0.20, 0.25\}$ and by repeating the concordance analysis with alternative block sizes of 5,000 and 20,000 consecutive zeros. The primary reported specification retained 10,000-zero zones and $\tau = 0.2$ because these values provide ten equally

sized regions and a direct microscopic-gap criterion. All formulas, thresholds, zone boundaries, and benchmark parameters were fixed before interpreting the zone-wise outcomes.

4.9 Spectral Analysis Output Framework

The methodology produces one zone-wise analytical record for each Z_k containing the zero-index range, mean unfolded spacing, Kolmogorov distance, ZSCI score, microscopic gap-anomaly rate, and five-level number variance. These outputs are subsequently used to test whether improved global GUE concordance is accompanied by the disappearance of local anomalies or whether both phenomena coexist. The latter pattern constitutes the proposed dual-scale spectral signature of ZETA-SPECTRAL and directly addresses the study objectives concerning spectral concordance, local spacing anomalies, rigidity, and zone-wise spectral evolution.

5. Results and Discussion

This section presents the numerical results obtained from the ZETA-SPECTRAL framework and interprets the spectral behaviour of the first 100,000 analysed Riemann zeta zeros. The results are organized around global GUE concordance, microscopic gap irregularity, unfolding stability, five-level number variance, and robustness under alternative analytical specifications. The combined findings are then integrated to evaluate the proposed dual-scale spectral signature.

5.1 Zone-Wise Spectral Concordance

Table 4. Zone-Wise Kolmogorov Distance and Zeta Spectral Concordance Index

Zone	Zero-index range	D_k	ZSCI (%)
Z1	1–10,000	0.02755	97.245
Z2	10,001–20,000	0.02225	97.775
Z3	20,001–30,000	0.02343	97.657
Z4	30,001–40,000	0.02058	97.942
Z5	40,001–50,000	0.01912	98.088
Z6	50,001–60,000	0.02079	97.921
Z7	60,001–70,000	0.02042	97.958
Z8	70,001–80,000	0.01861	98.139
Z9	80,001–90,000	0.01743	98.257
Z10	90,001–100,000	0.01897	98.103

Table 4 shows an overall strengthening of agreement between the empirical unfolded spacing distributions and the GUE benchmark. The ZSCI rises from 97.245% in Z_1 to 98.103% in Z_{10}, while the corresponding Kolmogorov distance decreases from 0.02755 to 0.01897. The endpoint difference represents a concordance gain of 0.858 percentage points. The largest ZSCI is observed in Z_9 at 98.257%, with the smallest Kolmogorov distance of 0.01743. The sequence is not strictly monotonic, as local reductions occur in Z_3, Z_6, and Z_{10}; however, the later zones remain predominantly above the initial-zone concordance level. The result therefore indicates progressive large-scale spectral alignment rather than a perfectly smooth convergence process.

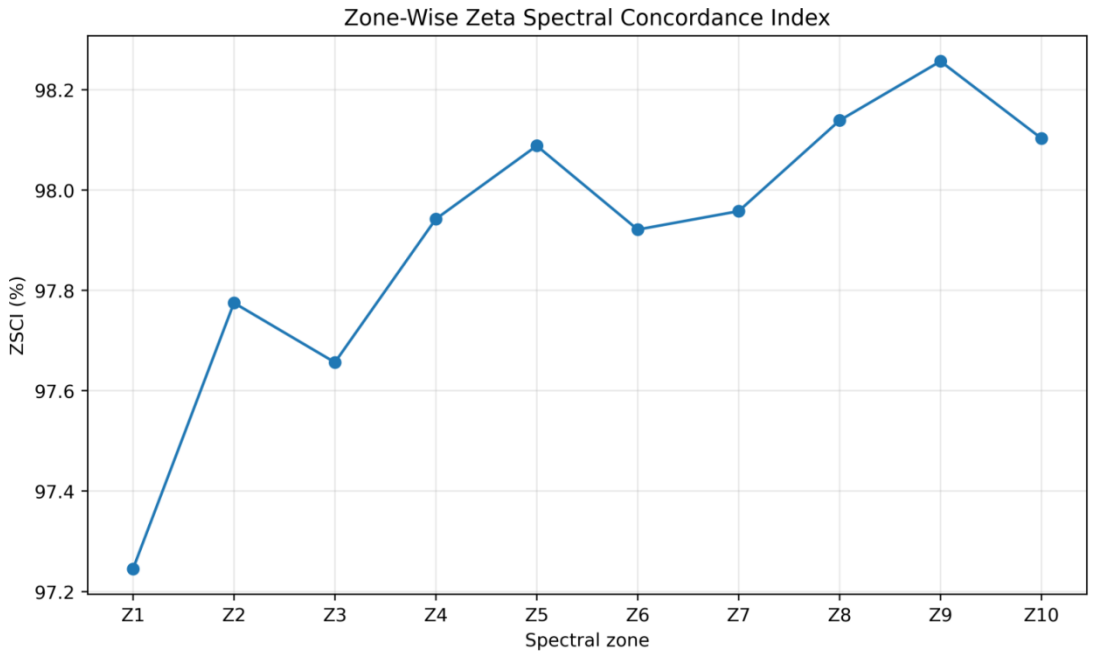

Figure 3. Zone-Wise Variation in the Zeta Spectral Concordance Index

Figure 3 highlights the upward shift in spectral concordance across the analysed zero regions. The rise from the early-zone level to the higher values in Z_8 and Z_9 is accompanied by small zone-specific reversals, indicating that the spectral sequence retains finite local fluctuations while showing stronger overall agreement with the selected GUE reference. This behaviour is consistent with the use of random-matrix statistics as a comparative description of local zeta-zero structure, while the proposed ZSCI provides a direct percentage-scale measure for consecutive zero blocks.

5.2 Microscopic Gap Anomalies and Unfolding Stability

Table 5. Zone-Wise Microscopic Gap-Anomaly Rate and Mean Unfolded Spacing

Zone	**$A_k(0.2)$ (%)**	**Mean unfolded spacing**
Z1	0.420	1.000023
Z2	0.610	0.999970
Z3	0.790	1.000091
Z4	0.590	0.999990
Z5	0.580	0.999998
Z6	0.490	0.999980
Z7	0.620	1.000046
Z8	0.640	0.999955
Z9	0.720	1.000001
Z10	0.670	0.999997

Table 5 summarizes the zone-wise microscopic gap-anomaly rate and mean unfolded spacing. The sub-0.2 gap-anomaly rate does not disappear as GUE concordance strengthens. The anomaly rate increases from 0.420% in Z_1 to 0.670% in Z_{10} and reaches its maximum value of 0.790% in Z_3. Later zones continue to contain compressed spacings, including rates of 0.640% in Z_8 and 0.720% in Z_9. At the same time, the mean unfolded spacing remains extremely close to unity in every zone, ranging from 0.999955 to 1.000091. The maximum

absolute departure from unit mean spacing is approximately 0.000091, supporting the numerical stability of the unfolding procedure. The persistence of small-gap events is therefore not explained by a failure of mean-density normalization.

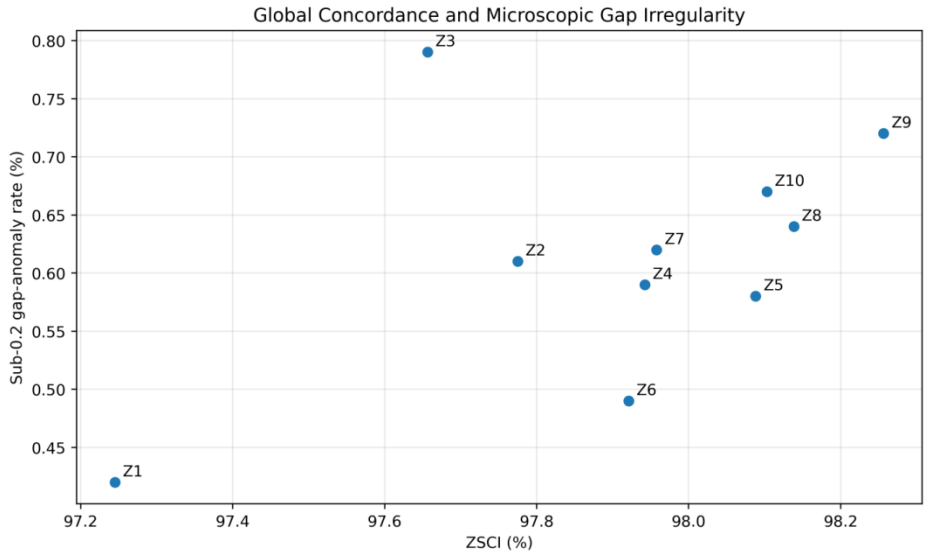

Figure 4. Global Spectral Concordance and Microscopic Gap Irregularity across the Ten Zones

Figure 4 provides the clearest numerical evidence for the proposed dual-scale behaviour. Zones with comparatively high ZSCI values continue to exhibit measurable sub-0.2 gap frequencies; notably, Z_9 records the highest concordance value of 98.257% together with an anomaly rate of 0.720%. Thus, stronger agreement of the complete spacing distribution with the GUE benchmark does not require the elimination of exceptionally compressed local spacings. The finding separates distribution-level organization from rare local events and extends the spectral interpretation beyond a single goodness-of-fit statistic.

5.3 Five-Level Number Variance and Spectral Rigidity

Table 6. Zone-Wise Five-Level Number Variance

Zone	Five-level number variance, $\Sigma^2_k(5)$	Interpretation
Z1	0.36368	Bounded multilevel fluctuation
Z2	0.39166	Bounded multilevel fluctuation
Z3	0.40082	Bounded multilevel fluctuation
Z4	0.40501	Bounded multilevel fluctuation
Z5	0.40901	Bounded multilevel fluctuation
Z6	0.40903	Bounded multilevel fluctuation
Z7	0.41372	Bounded multilevel fluctuation
Z8	0.41400	Bounded multilevel fluctuation
Z9	0.41559	Bounded multilevel fluctuation
Z10	0.41495	Bounded multilevel fluctuation

Table 6 summarizes the five-level number variance across the ten spectral zones. The five-level number variance remains below 0.418 in all ten zones. It increases from 0.36368 in Z_1 to 0.41495 in Z_{10} and reaches a maximum of 0.41559 in Z_9. The gradual increase indicates that the long-range counting fluctuation is not constant across the first 100,000 zeros; however, the restricted numerical range from 0.36368 to 0.41559 shows that all zones remain within a bounded multilevel fluctuation regime. Consequently, the results do not support a

claim of progressively increasing rigidity. Instead, they identify persistent spectral constraint accompanied by a mild height-dependent change in five-level counting variance.

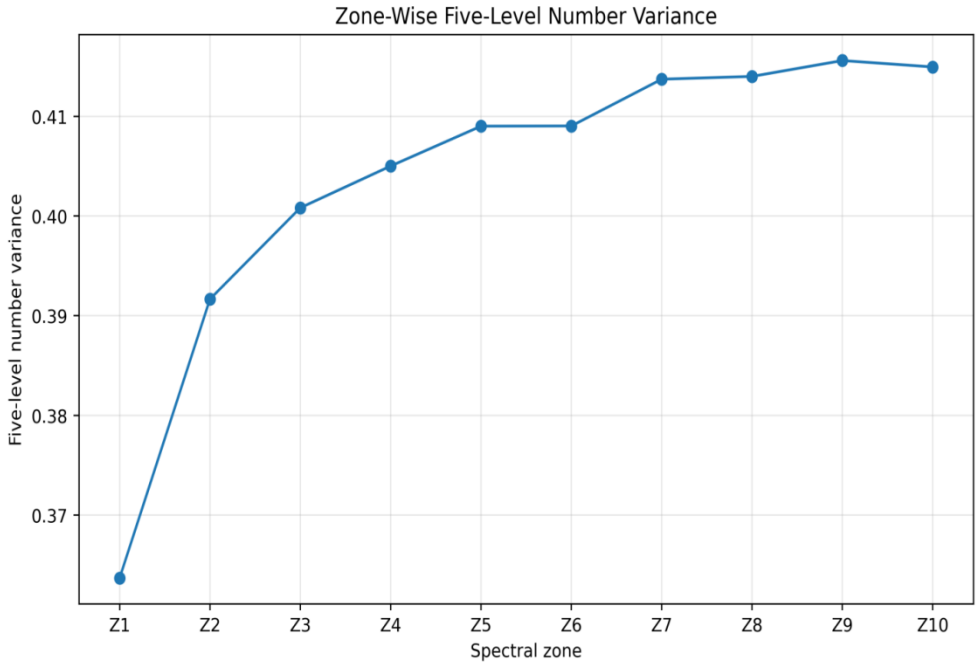

Figure 5. Five-Level Number Variance across Successive Spectral Zones

Figure 5 shows that most of the increase in number variance occurs between the early and middle zones, after which the values approach a narrower band near 0.41. The small reduction from 0.41559 in Z_9 to 0.41495 in Z_{10} further confirms that the zone-wise pattern is not strictly monotonic. This bounded but non-constant rigidity measure complements ZSCI by capturing a longer-range feature that cannot be inferred from nearest-neighbour spacing concordance alone.

5.4 Robustness Analysis

Table 7. Sensitivity of the Microscopic Gap-Anomaly Result to Alternative Thresholds

Threshold, τ	Z_1 anomaly rate (%)	Z_{10} anomaly rate (%)	Endpoint change (percentage points)
0.15	0.170	0.380	+0.210
0.20	0.420	0.670	+0.250
0.25	0.960	1.260	+0.300

Table 7 demonstrates that the endpoint persistence of microscopic gap anomalies is not specific to the primary threshold of 0.2. When the threshold is tightened to 0.15, the anomaly rate changes from 0.170% in Z_1 to 0.380% in Z_{10}. At the broader threshold of 0.25, the corresponding values are 0.960% and 1.260%. All three threshold specifications retain a positive endpoint difference, supporting the conclusion that compressed local spacings persist in the later zero region.

Table 8. Robustness of Endpoint ZSCI Gain under Alternative Spectral Block Sizes

Block size	Number of zones	Initial-zone ZSCI (%)	Final-zone ZSCI (%)	Concordance gain (points)
5,000 zeros	20	96.886	98.028	1.142
10,000 zeros	10	97.245	98.103	0.858

Block size	Number of zones	Initial-zone ZSCI (%)	Final-zone ZSCI (%)	Concordance gain (points)
20,000 zeros	5	97.586	98.239	0.653

Table 8 evaluates the robustness of the endpoint ZSCI gain under alternative spectral block sizes. The positive endpoint ZSCI gain is also preserved under alternative block sizes. Blocks of 5,000 zeros produce a gain of 1.142 percentage points, the primary 10,000-zero specification produces a gain of 0.858 points, and 20,000-zero blocks produce a gain of 0.653 points. Although the magnitude of the gain changes with the aggregation scale, the direction of the endpoint result remains unchanged. The principal spectral-concordance finding is therefore robust to the three tested segmentation scales**.**

5.5 Integrated Dual-Scale Spectral Signature

Table 9. Integrated Evidence for the ZETA-SPECTRAL Dual-Scale Signature

Diagnostic dimension	Initial region	Final/later-region evidence	Integrated interpretation
Global concordance	ZSCI = 97.245%	ZSCI = 98.103%; peak = 98.257%	Stronger overall GUE agreement
Microscopic irregularity	$A_1(0.2)$ = 0.420%	$A_{10}(0.2)$ = 0.670%; persistent in all zones	Compressed local gaps remain
Unfolding stability	Mean = 1.000023	Mean = 0.999997	Unit-mean normalization retained
Five-level rigidity	$\Sigma^2_1(5)$ = 0.36368	$\Sigma^2_{10}(5)$ = 0.41495; all < 0.418	Bounded multilevel fluctuation

Table 9 integrates the principal spectral indicators supporting the proposed ZETA-SPECTRAL dual-scale signature. The integrated results establish a dual-scale spectral signature in the analysed zero sequence. At the distribution level, the decrease in Kolmogorov distance and the 0.858-point endpoint increase in ZSCI indicate stronger GUE-like spacing concordance. At the microscopic level, sub-0.2 gap events remain present and show a larger endpoint frequency, even in zones with the strongest global concordance. Mean unfolded spacing remains effectively equal to one, while five-level number variance stays below 0.418. The numerical evidence therefore supports coexistence between large-scale spectral organization and persistent fine-scale irregularity rather than a transition toward uniform local spacing.

This finding complements recent spectral-flow and Hamiltonian interpretations by providing a direct block-wise diagnostic of the zero sequence rather than constructing a specific operator model (LeClair, 2025; Yakaboylu, 2024). The observed GUE-like concordance is also consistent with the wider random-matrix treatment of zeta-zero spacings, while the continued presence of compressed gaps shows why a single aggregate spacing statistic cannot fully describe local spectral geometry (Nishigaki, 2024; Nishigaki, 2026). Similarly, collective spectral measures can capture broad quantum-chaotic organization without necessarily isolating rare microscopic spacing events (Basu et al., 2026). ZETA-SPECTRAL therefore contributes an integrated descriptive framework that places global concordance, local anomalies, and multilevel variance on the same zone-wise analytical structure.

5.6 Discussion

The present study demonstrates that the Zeta Spectral Concordance Index increased from 97.245% in the first spectral zone to 98.103% in the final zone, with the highest value of 98.257% observed in Z_9. This progressive improvement in GUE-like concordance supports the statistical interpretation of Riemann zeta zeros as a highly organized spectral sequence. The finding is consistent with Nishigaki (2024), who demonstrated that consecutive level-spacing and gap-ratio statistics of Riemann zeros exhibit close relationships with Gaussian Unitary Ensemble behaviour. Similarly, Nishigaki (2026) reported that finite-size corrected unitary-ensemble statistics provide increasingly refined descriptions of high Riemann-zero spacings. Therefore, the present results extend earlier random-matrix comparisons by providing a zone-wise quantitative concordance measure that directly tracks changes in spectral agreement across successive zero regions.

The persistence of sub-0.2 microscopic gap anomalies provides a complementary interpretation of the zero spectrum. Although overall spectral concordance strengthens, the anomaly rate increases from 0.420% to 0.670%, demonstrating that compressed local spacings remain present within increasingly GUE-like spectral zones. This result is consistent with Goldston et al. (2023), who emphasized the complexity of unusually small consecutive gaps and the limitations of classical methods for characterizing extreme spacing behaviour. The present finding also complements Basu et al. (2026), whose spectral form-factor analysis identified collective quantum-chaotic organization but did not directly isolate rare microscopic spacing events. Thus, ZETA-SPECTRAL shows that global spectral organization and local irregularity are not mutually exclusive and may coexist within the same ordered sequence of Riemann zeta zeros.

The stable mean unfolded spacing and five-level number variance below 0.418 further support the reliability of the proposed dual-scale interpretation. The near-unit mean spacing confirms that the unfolding procedure effectively removes the large-scale variation in zero density, while the bounded number variance indicates constrained multilevel fluctuations across the ten spectral zones. These observations are compatible with the broader spectral and zero-density perspectives reported by Bellotti (2025) and Guth and Maynard (2026), which emphasize increasing quantitative control over the organization of zeta zeros at large heights. However, unlike global density estimates, the present study simultaneously evaluates distributional concordance, microscopic gap anomalies, and multilevel rigidity. Collectively, the results establish ZETA-SPECTRAL as an integrated analytical framework for describing the coexistence of large-scale spectral stabilization and persistent fine-scale irregularity in the first 100,000 analysed Riemann zeta zeros.

6. Conclusion

The present study introduced ZETA-SPECTRAL, a unified computational spectral framework for examining non-trivial Riemann zeta zeros through global concordance, microscopic spacing irregularity, and multilevel spectral rigidity. Analysis of the first 100,000 critical-line zeros showed that the Zeta Spectral Concordance Index increased from 97.245% in Z_1 to 98.103% in Z_{10} and reached a maximum of 98.257% in Z_9. At the same time, the sub-0.2 gap-anomaly rate changed from 0.420% to 0.670%, demonstrating that compressed local gaps persisted even as overall GUE-like agreement strengthened. The mean unfolded spacing remained extremely close to unity, while five-level number variance remained below 0.418, supporting stable normalization and bounded multilevel spectral fluctuations.

These findings establish the proposed dual-scale spectral signature, in which large-scale spectral organization coexists with persistent microscopic irregularity. The proposed ZSCI, zone-wise spectral segmentation, and integrated multiscale diagnostics extend existing spectral and random-matrix interpretations by providing a direct quantitative framework for comparing successive regions of the zeta-zero sequence. ZETA-SPECTRAL therefore offers a reproducible analytical approach for investigating hidden spectral structure in Riemann zeros and may support future comparison of Hamiltonian, Hilbert–Pólya, quantum-scattering, and other operator-based models.

Limitation

The study is limited to the first 100,000 critical-line Riemann zeta zeros and the selected GUE-based spectral diagnostics.

Future work

Further studies may extend the framework to substantially higher zero ordinates, alternative random-matrix benchmarks, and explicit self-adjoint operator constructions.

Data and Code Availability

The zero ordinates analysed in this study are publicly available from Andrew Odlyzko's table of the first 100,000 zeros of the Riemann zeta function (Odlyzko, n.d.). The analysis code and zone-wise numerical outputs should be archived as supplementary files with the final submission to support exact reproducibility.

References

1. Assiotis, T. (2022). Random entire functions from random polynomials with real zeros. Advances in Mathematics, 410, 108701. https://doi.org/10.1016/j.aim.2022.108701.
2. Basu, P., Das, S., & Krishnan, C. (2026). An analytic zeta function ramp at the black hole Thouless time. Journal of High Energy Physics, 2026, 2. https://doi.org/10.1007/JHEP02(2026)002.
3. Bellotti, C. (2024). Explicit bounds for the Riemann zeta function and a new zero-free region. Journal of Mathematical Analysis and Applications, 536(2), 128249.
4. Bellotti, C. (2025). An explicit log-free zero density estimate for the Riemann zeta-function. Journal of Number Theory, 269, 37–77.

5. Bianchi, M., Firrotta, M., Sonnenschein, J., &Weissman, D. (2024). From spectral to scattering form factor. arXiv preprint arXiv:2403.00713.
6. Chen, Z. (2024). Non-Abelian observable-geometric phases and the Riemann zeros. arXiv preprint arXiv:2403.19118.
7. Curran, M. J. (2021). Upper bounds for fractional joint moments of the Riemann zeta function. ActaArithmetica, 204(1), 83–96.
8. Curran, M. J. (2024). Freezing transition and moments of moments of the Riemann zeta function. The Quarterly Journal of Mathematics, 75(4), 1481–1505. https://doi.org/10.1093/qmath/haae055.
9. Giordano, F., Negro, S., &Tateo, R. (2023). The generalised Born oscillator and the Berry–Keating Hamiltonian. arXiv preprint arXiv:2307.15025.
10. Goldston, D. A., Trudgian, T. S., &Turnage-Butterbaugh, C. L. (2023). On the Montgomery–Odlyzko method regarding gaps between zeros of the zeta-function. Journal of Mathematical Analysis and Applications, 527(2), 127548.
11. Guth, L., & Maynard, J. (2026). New large value estimates for Dirichlet polynomials. Annals of Mathematics, 203(2), 623–675.
12. Hartnoll, S. A., & Yang, M. (2025). The conformal primon gas at the end of time. Journal of High Energy Physics, 2025, 281. https://doi.org/10.1007/JHEP07(2025)281.
13. Heap, W., &Soundararajan, K. (2022). Lower bounds for moments of zeta and L-functions revisited. Mathematika, 68(1), 1–14.
14. Hedenmalm, H. (2026). Spectral interpretation of Riemann zeta zeros. arXiv preprint arXiv:2606.17494.
15. Inoue, S., Kobayashi, H., &Toma, Y. (2026). Explicit extreme values of the argument of the Riemann zeta-function. Mathematical Proceedings of the Cambridge Philosophical Society, 1–15. https://doi.org/10.1017/S0305004126102060.
16. Kovaleva, V. (2024). Correlations of the squares of the Riemann zeta on the critical line. arXiv preprint arXiv:2401.13725.
17. LeClair, A. (2025). Spectral flow for the Riemann zeros. Advances in Theoretical and Mathematical Physics, 29(4), 1125–1156.
18. LeClair, A., &Mussardo, G. (2024). Riemann zeros as quantized energies of scattering with impurities. Journal of High Energy Physics, 2024, 62. https://doi.org/10.1007/JHEP04(2024)062.
19. Mine, M. (2026). Connection between the Riemann zeta-function and random matrices via hyperfunctions. arXiv preprint arXiv:2606.07312.
20. Mossinghoff, M. J., Trudgian, T. S., & Yang, A. (2024). Explicit zero-free regions for the Riemann zeta-function. Research in Number Theory, 10, 11.
21. Ng, N., Shen, Q., & Wong, P.-J. (2024). Shifted moments of the Riemann zeta function. Canadian Journal of Mathematics, 76(5), 1556–1586. https://doi.org/10.4153/S0008414X23000548.
22. Nishigaki, S. M. (2024). Distributions of consecutive level spacings of Gaussian unitary ensemble and their ratio: Ab initio derivation. Progress of Theoretical and Experimental Physics, 2024(8), 081A01. https://doi.org/10.1093/ptep/ptae120.
23. Nishigaki, S. M. (2026). Distributions of consecutive level spacings of circular unitary ensemble and their ratio: Finite-size corrections and Riemann ζ zeros. Progress of Theoretical and Experimental Physics, 2026(2), 023A02. https://doi.org/10.1093/ptep/ptag006.
24. Odlyzko, A. M. (n.d.). Tables of zeros of the Riemann zeta function. University of Minnesota.
25. Pei, Z. (2025). Riemann zeros and the KKR determinant. arXiv preprint arXiv:2504.07928.
26. Suo, X. (2025). On the Hamiltonian with energy levels corresponding to Riemann zeros. arXiv preprint arXiv:2505.21192.
27. Tamburini, F. (2025). A Majorana relativistic quantum spectral approach to the Riemann Hypothesis in (1+1)-dimensional Rindlerspacetimes. arXiv preprint arXiv:2503.09644.
28. Yakaboylu, E. (2024a). Hamiltonian for the Hilbert–Pólya conjecture. Journal of Physics A: Mathematical and Theoretical, 57(23), 235204. https://doi.org/10.1088/1751-8121/ad4c2d.
29. Yakaboylu, E. (2024b). Nontrivial Riemann Zeros as Spectrum. arXiv preprint arXiv:2408.15135.
30. Yang, A. (2024). Explicit bounds on ζ(s) in the critical strip and a zero-free region. Journal of Mathematical Analysis and Applications, 534(2), 128124.
31. Yu, S., Piao, X., & Park, N. (2024). Computing Riemann zeros with light scattering. arXiv preprint arXiv:2408.01095.